# Electron-spectroscopic study of vertical $In_{1-x}Ga_xAs$ quantum dots

J. W. Sleight,* E. S. Hornbeck, M. R. Deshpande, R. G. Wheeler, and M. A. Reed
*Departments of Applied Physics, Electrical Engineering, and Physics, Yale University, P.O. Box 208284, New Haven, Connecticut 06520*

R. C. Bowen and W. R. Frensley
*Eric Jonsson School of Engineering, University of Texas, Dallas, P.O. Box 830688, Richardson, Texas 75083*

J. N. Randall and R. J. Matyi†
*Central Research Laboratories, Texas Instruments Incorporated, Dallas, Texas 75265*
(Received 24 May 1995; revised manuscript received 8 December 1995)

We present the results of a magnetotransport study of vertical $In_{1-x}Ga_xAs$ quantum dots. We observe a series of current plateaus, due to the quantum dot eigenstates, that exhibit a purely diamagnetic response in magnetic field parallel to the current, and no shift in energy in magnetic field perpendicular to the current. In perpendicular field, a suppression of the current plateaus is observed that is not present in parallel field. We also observe fine structure on the current plateaus and study its magnetic field dependence. We observe that the fine structure moves systematically in voltage with changing magnetic field, in both the perpendicular and parallel field orientations, while the plateau edges only exhibit a diamagnetic shift in parallel field. The current plateau step edge exhibits the expected Fermi-level broadening with temperature whereas the fine structure is observed to be relatively temperature insensitive. This is indicative of tunneling from states in the emitter below the Fermi level. Additionally, thermal activation of subthreshold fine structure is observed. We attribute the origin of this fine structure to the dopant-induced discreteness of the electronic density of states in the emitter.

## I. INTRODUCTION

Tunneling in low-dimensional semiconductor structures has been a very active research field, both experimentally[1–9] and theoretically.[10–18] Electron confinement is usually achieved either through fabrication imposed confinement of a double-barrier resonant-tunneling structure (DBRTS) or through electrostatic confinement of a two-dimensional (2D) electron layer. Both techniques create a potential that spatially localizes an electron in a region, the dot, and quantize the allowed energy levels in this region. These two techniques also allow for the coupling of electrodes to the sample. One electrode, the emitter, probes the density of quasi-0D states by injecting electrons into the dot. The other electrode, the collector, allows injected electrons to leave the dot.

In the case of 2D electron layers that are electrostatically confined, the single-electron charging energy, $U_C$, is usually much greater than $\delta E$, the spacing between single-particle states in the dot. In the case of a double-barrier semiconductor heterostructure, $\delta E$ and $U_C$ can be of the same order,[2] or $U_C$ can be less than $\delta E$. In the regime where they are on the same order, it is difficult to distinguish between the transport phenomena caused by each of these effects[2,16] and proper modeling[14] is required to appropriately assign the observed structure to either spatial quantization or single-electron charging.

Much of the previous work in double-barrier structures utilizes a GaAs well between two $Al_xGa_{1-x}As$ barriers to form the dot.[1,2,5,9] Typically, the well and barriers are undoped. Undoped spacer layers ($\sim$100 Å) are situated immediately prior to the barriers to prevent the diffusion of dopants into the $Al_xGa_{1-x}As$ barriers during growth. Dopants in $Al_xGa_{1-x}As$ are known to form deep donor levels (*DX* centers), and it is preferable to avoid complicating the electron spectroscopy with events due to these levels.[19] These spacer layers are usually contacted by highly doped GaAs. This results in a conduction-band profile for the bulk epitaxial material as shown in Fig. 1(a).[20] The first quantized state in the well is relatively far away from the Fermi level in the emitter, due to band bending in the spacer layer region (lateral quantization pulls the dot states up even further). In this example, biases on the order of hundreds of millivolts are needed to pull these states down and to inject electrons into the dot. By using an $In_{1-x}Ga_xAs$ well, the equilibrium dot quantum states may be brought down closer to, or below, the Fermi level [Fig. 1(b)]. Lower quantum levels in the well imply longer lifetimes (i.e., less intrinsic energy broadening). Additionally, since this reduces the resonant bias voltage, far less distortion of the emitter-dot-collector potential occurs while examining the density of states of the dot, as compared to a conventional GaAs vertical quantum dot. Due to the lower applied bias required, there is far less power dissipation and local electron heating in the dot region.

## II. SAMPLE GROWTH AND FABRICATION

Samples are grown using molecular-beam epitaxy on a Si-doped (100) GaAs substrate. The active region consists of a 50-Å $In_{0.1}Ga_{0.9}As$ quantum well, enclosed by a pair of 40-Å-thick $Al_{0.25}Ga_{0.75}As$ barriers. This region, along with 100-Å spacer layers of GaAs that contact the barriers, is undoped. The spacer layers are contacted by GaAs doped with Si at a density of $3\times10^{18}$ cm$^{-3}$.

Small ($\sim$100 nm) AuGe/Ni/Au Ohmic top-contact dots

 © 1996 The American Physical Society

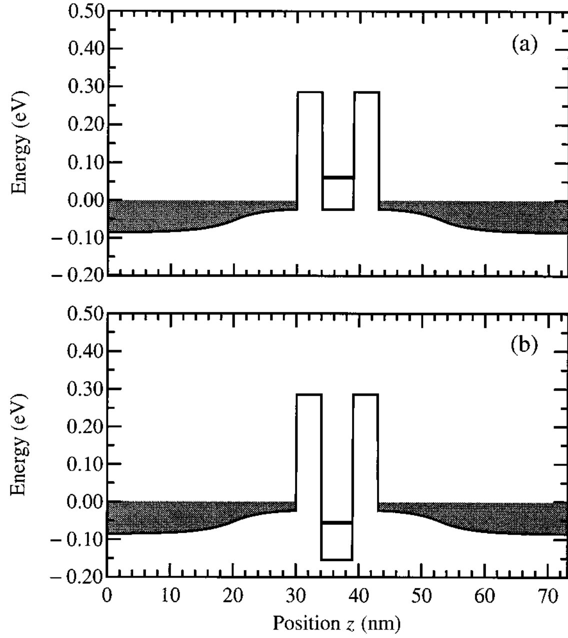


FIG. 1. Conduction band diagram in the tunneling direction for (a) a GaAs quantum well (unconfined laterally) and the corresponding diagram for (b) an $In_{0.1}GaAs_{0.9}$ quantum well. The shaded regions correspond to occupied electron states below the Fermi level and the line in the well denotes the position of the ground-state level.

are defined by electron-beam lithography on the surface of the grown resonant tunneling structure. A bilayer polymethylmethacrylate resist and lift-off method is used. The metal dot Ohmic contact serves as a self-aligned etch mask for highly anisotropic reactive ion etching (RIE) using $BCl_3$ as an etch gas. The resonant tunneling structure is etched through to the bottom $n^+$ GaAs contact. Contact to the top of the structures is achieved through a planarizing-etchback process employing polyimide and an $O_2$ RIE.[3] A gold contact pad is then evaporated over the columns. Bottom contact is achieved through the conductive substrate.

## III. THEORY

### A. Lateral quantization and magnetic field

Consider a quantum well that has been quantized in the vertical dimension through epitaxial growth. The vertical confinement in such a structure is modeled by a rectangular potential. In the lateral dimension through fabrication, we can create a system that is a quasi-0D dot connected to the outside world by two 1D leads. The lateral confinement, which is enhanced due to Fermi-level pinning at midgap on the sidewalls, may be modeled by a parabolic potential.[2,3]

For a parabolic model the allowed energy levels, $E_{n,\ell}$, are given by $(2n+|\ell|+1)\hbar\omega_0$, where the radial quantum numbers $n=0,1,2,\ldots$, the azimuthal quantum numbers $\ell=0,\pm1,\pm2,\ldots$, and $\hbar\omega_0$ is the energy state spacing in the parabolic well. $E_0$, the energy spacing between states, $\Delta E=\hbar\omega$, is $(2\Phi_T/m^*)^{(1/2)}(\hbar/R)$, where $\Phi_T$ is the Fermi-level pinning energy at the sidewalls, $R$ is the lateral physical dimension, and $m^*$ is the electron effective mass. For a GaAs well, with $Al_xGa_{1-x}As$ barriers, typical values for energy state separation are on the order of 25 meV, for $\Phi_T=0.8$ eV and $R\approx500$ Å.

If a magnetic field oriented parallel to the current is applied, according to first-order perturbation theory, the shift of the energy levels is given by

$$\delta E_{B\parallel I}=\left(\frac{e\hbar}{2m^*}\right)\ell B+\frac{e^2B^2\langle r_0^2\rangle}{8m^*}. \tag{1}$$

Note that spin is neglected in Eq. (1), as the spin splitting energy, $ge\hbar B/2m$, is only 0.25 meV at 10 T. The shift for a localized level with $\ell=0$ is *entirely* due to the diamagnetic term, $\delta E_{\text{diamag}}=e^2B^2\langle r_0^2\rangle/8m^*$, where $\langle r_0^2\rangle$ is the spatial extent of the localized wave function. Therefore, the observation of an experimental diamagnetic shift is a *direct measure* of $\langle r_0^2\rangle$.

For magnetic field oriented perpendicular to the current, the first-order perturbation term is more difficult to evaluate, and numerical methods are required.[21,22] Numerical results indicate an increase in dot energy states by a diamagnetic shift term, which is predicted to be less than 0.5 meV at 10 T for a $GaAs/Al_xGa_{1-x}As$ quantum dot system with the same well width (50 Å) as in this study. The small value for the state energy shift in this field orientation is due to the interaction of a relatively weak magnetic potential with the much stronger confinement potential in the epitaxial confinement $(z)$ direction.

### B. Charging effects

Charging effects become important as the lateral device area is scaled down. Charging can be introduced into the usual single-electron model, by modeling the Coulomb charging energy of the quantum dot as arising from a single effective capacitance $C$.[1] This approach uses the semiclassical geometric capacitance (the sum of an emitter capacitance $C_e$ and a collector capacitance $C_c$),

$$C=C_e+C_c\approx\frac{\epsilon\epsilon_0\pi a^2}{4}(d_e^{-1}+d_c^{-1}), \tag{2}$$

where $d_e$ and $d_c$ are the thicknesses of the emitter and collector barriers, respectively, and $a$ is the dot effective electrical diameter. For the structures in this paper, $C\approx2.6\times10^{-16}$ F using $\epsilon_{Al_xGa_{1-x}As}\approx11.6$, and $a\approx800$ Å. The value $a$ is the electrical diameter, which is the extrapolated value determined from current density measurements on large area samples. In this case, the estimated charging energy, $E_C=e^2/2C$, is approximately 0.31 meV.[23] More generally, $E_{C,N}=e^2/C(N-1/2)$ is the Coulomb charging energy for $N$ electrons residing on the dot.[1,24]

### C. Numerical results

While many of the analytic results are very useful to first order in determining expected diamagnetic shifts and state spacings, the treatment of the lateral potential as either a parabolic or hardwall potential is an oversimplification of the problem. In order to treat the *real* lateral potential, numerical 3D potential models have been pursued to more accurately

determine the expected level spacings and diamagnetic shifts. Starting from a physical description of the structure, the Poisson equation is solved self-consistently using a nonlinear successive over-relaxation algorithm.[10] Zero-field boundary conditions are invoked at the $z$ boundaries and the azimuthal axis. The electrostatic potential at the surface is chosen such that the Fermi level is pinned near midgap. It is assumed that the pinning in the well and barrier is determined by the pinning in the GaAs.

The energy eigenstates within the 0D dot are determined by numerically solving the Schrödinger equation in cylindrical coordinates,

$$-\frac{\hbar^2}{2m^*}\left[\frac{1}{r}\frac{\partial}{\partial r}\left(r\frac{\partial\psi}{\partial r}\right)+\frac{1}{r^2}\frac{\partial^2\psi}{\partial\phi^2}+\frac{\partial^2\psi}{\partial z^2}\right]+V\psi=E\psi. \quad (3)$$

Invoking the separation of variables $\psi(r,\phi,z)=R(r,z)\Phi(\phi)$ and substitution of the radial function $u(r,z)=\sqrt{r}R(r,z)$ reduces Eq. (3) to the following form for cylindrically symmetric potentials:

$$-\frac{\hbar^2}{2m^*}\left[\nabla_r^2+\nabla_z^2+\frac{1}{r^2}\left(\ell^2-\frac{1}{4}\right)\right]u+V(r,z)u=Eu, \quad (4)$$

where $\ell$ is the azimuthal angular momentum. This equation is discretized on a finite difference basis resulting in a symmetric pentadiagonal Hamiltonian matrix. A hard wall boundary is invoked at the external edges of the $Al_xGa_{1-x}As$ barriers and the exposed surface. The eigenstates are calculated using a shift and invert Lanczos algorithm followed by inverse iteration.[25] Results from these calculations are used to determine the energy spacing between quantized levels ($\Delta E$).

Choosing the scalar potential $\mathbf{A}=(1/2)(\mathbf{B}\times\mathbf{r})$, the electronic potential due to a magnetic field parallel to the current ($z$ direction) is given by

$$V_{B_z}(r,z)=\frac{1}{2m^*}\left[\frac{e^2}{4}B^2r^2+e\hbar B\ell\right]. \quad (5)$$

The addition of this term to the Hamiltonian allows for the calculation of the dot eigenstate magnetic field dependence.

## IV. EXPERIMENTAL RESULTS

Several different types of transport measurements were performed to investigate the electronic properties of the vertical $In_xGa_{1-x}As$ quantum dot structures. First, large area samples (i.e., no lateral confinement) were examined to verify the epitaxial ($z$) potential and to determine current densities in the bulk material. Following this, small area dot structures were measured at low temperatures. Variable temperature data, as well as a variety of magnetotunneling measurements will be presented.

### A. Large area samples

Large area resonant tunneling diodes are fabricated to examine the peak positions and current densities for the epitaxial material. Figure 2(a) shows a current versus voltage trace for a 1024-$\mu m^2$ sample measured at 4 K. The symmetric response is consistent with the symmetric epitaxial structure. The negative differential resistance occurs at $\pm 23$ mV with a peak current density of 56 A/cm$^2$. The low bias conductance is 25 mS for the 1024-$\mu m^2$ device, and this value is observed to scale linearly with device area, as expected, providing a means of extrapolating the upper limits for the electrical sizes of the smaller devices.

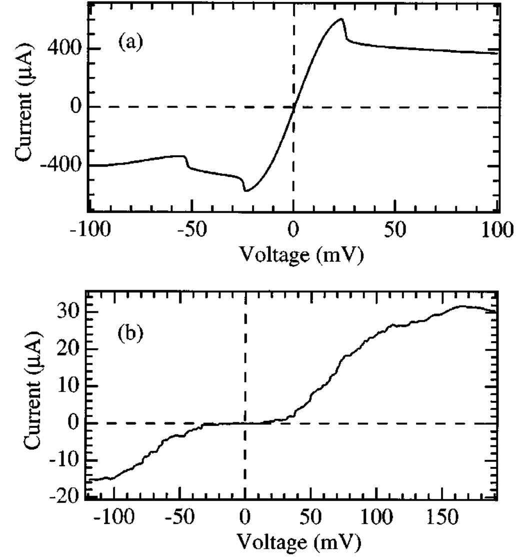


FIG. 2. (a) Current vs voltage for a large area (1024 $\mu m^2$) sample fabricated from the same epitaxial material used for the small area quantum dots ($T=4.2$ K); (b) current versus voltage for an $In_{0.1}Ga_{0.9}As$ quantum dot. Note the steplike structure in current near zero bias ($T=50$ mK, mixing chamber).

### B. Zero-magnetic-field measurements: small area samples

The small area quantum dot samples are measured at milliKelvin temperatures in a dilution refrigerator. Figure 2(b) shows a current versus voltage [$I(V)$] curve for a sample ($R\approx 100$ nm) under zero magnetic field, at a mixing chamber temperature of 50 mK. Figure 3 shows an expansion of the zero bias region. The conductance for this sample ($\sim$ 0.4 $\mu$S) yields a value of approximately 800 Å for the electrical diameter $a$.

A staircase structure in current is observed in Figs. 2(b) and 3 in both bias directions, especially at low biases.

Similar structure in the low bias regime for DBRTS has been previously reported by other groups.[2,26] The major dif-

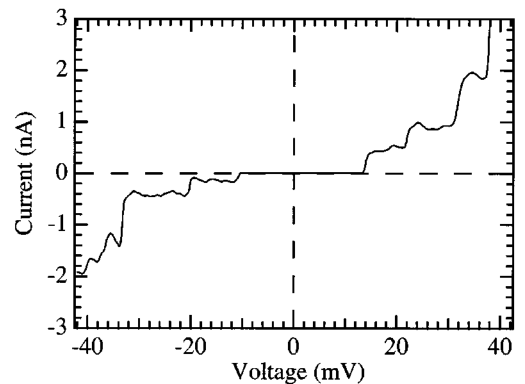


FIG. 3. An expansion of the low bias regime of Fig. 2(b).

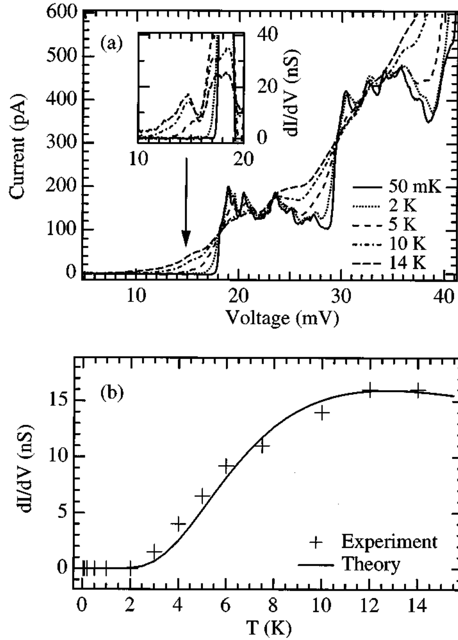


FIG. 4. (a) Reverse bias current vs voltage for a quantum dot at 35 mK, 2.0 K, 4.0 K, 5.0 K, 7.5 K, 10.0 K, and 14.0 K. The inset shows the subthreshold peak (in conductance) that arises as temperature is increased. (b) Experimental conductance (crosses) vs temperature [for the peak in the inset of (a)] and the theoretical fit (solid line).

ference in our work is the use of an $In_{1-x}Ga_xAs$ dot, as well as the use of a symmetric epitaxial structure. The current steps are relatively flat at low bias, where the transmission coefficient is not a strong function of applied bias. In order to analyze the electron spectroscopy in greater detail, we need to determine the bias to energy conversion factor, $\alpha$. The value of $\alpha$ is a measure of the amount of voltage that is actually dropped between the emitter and the quantum dot state. As will be shown, $\alpha$ may be determined from the temperature dependence of the plateau edges.

### C. Variable temperature measurements

The sharpness of the current plateau edges is expected to broaden as temperature increases, due to the broadening of the emitter Fermi distribution at higher temperature. The current versus voltage characteristics as a function of temperature for reverse bias are shown in Fig. 4(a). As expected, the plateau edges are very sensitive to changes in temperature.

The voltage to energy conversion factor, $\alpha$, is calculated from fitting the Fermi function to the first current plateau ($I_0$ is the value of the current on the plateau) in the variable temperature data, i.e.,

$$I(V,T)=I_0 f(\alpha V)=\frac{I_0}{1+\exp[-e\alpha(V-V_{\mathrm{th}})/(kT)]}. \tag{6}$$

$V_{\mathrm{th}}$ is threshold voltage for the current plateau and can be accurately determined from the intersection point of the $I(V,T)$ curves in Fig. 4(a), since the current given by Eq. (6) does not depend upon temperature for $V=V_{\mathrm{th}}$. The value of $\alpha$ is determined to be 0.37 meV/mV in the forward bias direction and 0.50 meV/mV in the reverse bias direction. The different $\alpha$ values imply an asymmetry in the emitter and collector contacts of the quantum dot device (either in doping, or in the barrier or spacer layer thickness) in contrast to the symmetric response seen in the large area device [Fig. 2(a)]. This is not surprising as we are now probing a very localized region instead of averaging over nonuniformities in barriers or series doping, as in the large area device.

It should also be noted that only temperatures *greater* than 1 K were used in determining $\alpha$, since below 1 K, the line shape can reach either the intrinsic linewidth that is limited by inelastic scattering[26] or the temperature limit for cooling the electrons in the dilution refrigerator. The electron temperature in the sample is often not the same as that of the mixing chamber, or of the sample thermometer, at milliKelvin temperatures. In both the reverse and forward bias directions, the sample's electrons appear to stop cooling at a mixing chamber temperature of 100–200 mK. This places an upper limit on the intrinsic state linewidth ($\Gamma$ at $T=0$) of approximately $1.9\times10^{-11}$ s.

Equation (6) predicts that the current value at the threshold point ($V=V_{\mathrm{th}}$) for the different temperature $I(V)$ curves in Fig. 4(a) should be $I_0/2$, half that of the plateau current, $I_0$. However, in both bias directions, the experimentally observed plateau current is less than $I_0$, typically only 75% of $I_0$. Equation (6) relies on the assumption of a constant density of states in the 1D emitter as the bias is increased. If we are near a 1D subband edge at $V=V_{\mathrm{th}}$, as the bias is increased the density of states, and current, will decrease. We also observe an oscillatory fine structure on the current plateaus which could affect the plateau current value. For this reason, $\alpha$ is determined by fitting the region where $V\leqslant V_{\mathrm{th}}$.

The observed fine structure between plateau edges [Fig. 4(a)] exhibits significantly less dependence upon temperature, especially for those peaks located far away from the plateau edges. This relative temperature insensitivity indicates tunneling of the electrons below the emitter Fermi level, where the emitter state occupation is not a strong function of temperature. Therefore, the fine structure is attributed to emitter states below the Fermi level, which pass into and out of resonance with the narrow 0D dot levels, as the applied bias is varied. At very low temperatures, only states in the emitter at or below the Fermi level, $E_F$, are occupied. These are the only emitter states available for tunneling. Electrons in the states nearest to the Fermi level will tunnel into the dot state first. States below the Fermi level then contribute to the tunneling as the bias is increased.

At finite temperature, occupation of the emitter states above the Fermi level is possible and therefore thermally activated resonances *below* the first plateau should be observed. The inset of Fig. 4(a) shows such a resonance effect, resulting in a subthreshold thermally activated conductance peak. Since $I(V)=I_0 f(\alpha V)$, where $I_0$ is a constant prefactor dependent upon the transmission coefficient, and $f(\alpha V)$ is the Fermi function, the conductance, $dI/dV=I_0 df(\alpha V)/dV$. A fit of this to the subthreshold conductance peak strength [inset Fig. 4(a)], assuming an emitter state above the Fermi level becomes thermally activated, is shown in Fig. 4(b). The energy difference between the thermally activated emitter state and Fermi level (1.7 meV) is

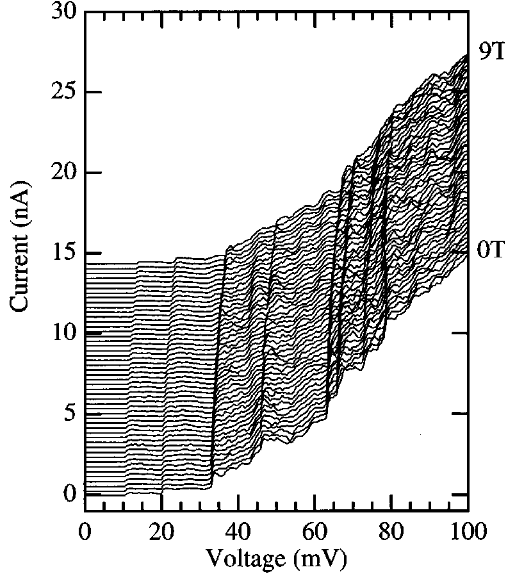


FIG. 5. Current-voltage characteristics in magnetic field parallel (0–9 T in 0.1875-T steps) to the current for the reverse bias direction. Traces are offset by a constant current value for clarity.

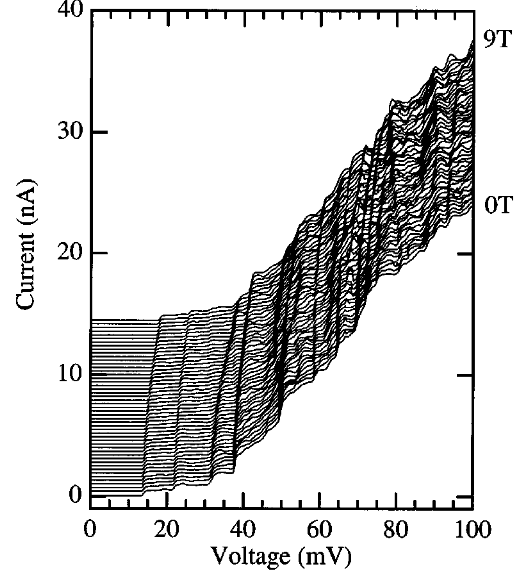


FIG. 6. Current-voltage characteristics in magnetic field parallel (0–9 T in 0.1875-T steps) to the current for the forward bias direction. Traces are offset by a constant current value for clarity.

known from measuring the difference between the plateau threshold voltage at low temperature (which determines the emitter Fermi-level position) and the thermally activated conductance peak position at higher temperatures. The *only* fitting parameter is $I_0$, which is within 5% of the value used for the first reverse bias current plateau (at $V=V_{th}$). A similar thermally activated subthreshold peak is observed in the forward bias direction as well.

### D. Magnetotunneling measurements

Two types of magnetotunneling measurements were performed. The first, which are discussed in this section, are measurements that include a large bias range [similar to that in Fig. 2(b)], over relatively large magnetic field increments (approximately 0.2 T) from 0 to 9 T. Both bias directions are covered, in magnetic field both parallel and perpendicular to the current (i.e., perpendicular and parallel to the quantum well, respectively). In order to better characterize the magnetoconductance of the fine structure on the plateaus, a low bias region ($\sim \pm 45$ mV) that contains the first few steps (similar to that shown in Fig. 3) is examined with higher current sensitivity and smaller magnetic field steps (approximately 0.02 T) for both bias directions and field orientations. This data are discussed in Sec. IV G.

In a magnetic field parallel to current, diamagnetic shifts of the dot ground-state levels are expected (see Sec. III A). Figures 5 and 6 show the reverse and forward current-voltage characteristics in magnetic field parallel to current, ranging from 0 to 9 T. The mixing chamber temperature is 30 mK and the step in magnetic field between traces is 1875 G. The traces are offset by a constant current value for clarity.

Note that there is a diamagnetic movement of all steps to higher bias with the magnetic field parallel to the current. This movement can be better observed in the fan diagram shown in Fig. 12, which will be presented in Sec. IV G. Plots of the plateau energy shift versus magnetic field squared (not shown) yield straight lines for all plateaus. At 9 T, the diamagnetic shift is approximately +1.4–2.6 meV (+2–4 mV), depending on the current step-dot level. Table I lists the values for the diamagnetic shifts and current plateau widths for the first six steps in reverse and forward bias directions. From Eq. (1) ($\ell=0$) and slope of the experimentally measured diamagnetic energy shift versus $B^2$ (accounting for $\alpha$), the radial wave-function extent is determined to be approximately 100 Å for the ground state in both bias directions. The implications of the radial wave-function extent upon the dot electron spectroscopy will be elaborated upon after discussing the results for the magnetic field oriented perpendicular to the current.

It should be noted here that all resonances shift to *higher* bias with *only* a diamagnetic trend. This is in contrast to the single-electron theories for two-dimensionally and three-dimensionally confined, nearly cylindrical quantum dots in a magnetic field.[27] These theories show that some states increase in energy with magnetic field, while other states decrease in energy. Starting from zero field, the ground state *always* shifts upward in energy, while the second state *always* shifts downward (ignoring spin). This is due to the

TABLE I. Experimentally observed diamagnetic shifts and current plateau widths for the reverse and forward bias directions.

| Plateau index ($N$) | $\delta E_{\text{diamag}}$ (meV, $B=9$ T) (reverse, forward bias) | Plateau width (meV) (reverse, forward bias) |
|---|---|---|
| 1 | 1.4,1.6 | 5.0,3.3 |
| 2 | 1.5,1.6 | 6.5,3.3 |
| 3 | 1.9,2.6 | 6.5,2.6 |
| 4 | 2.0,1.6 | 9.0,4.4 |
| 5 | 2.1,1.6 | 1.1,3.0 |
| 6 | 2.1,1.0 | 3.5,2.2 |

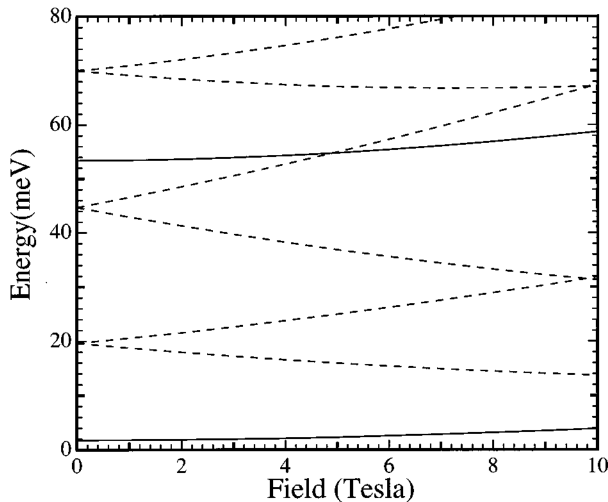


FIG. 7. Calculation of the energy eigenstate dependence upon magnetic field parallel to the current. The solid lines denote the $\ell=0$ states, the dashed lines denote the $\ell>0$ states, for a dot radius of 60 nm.

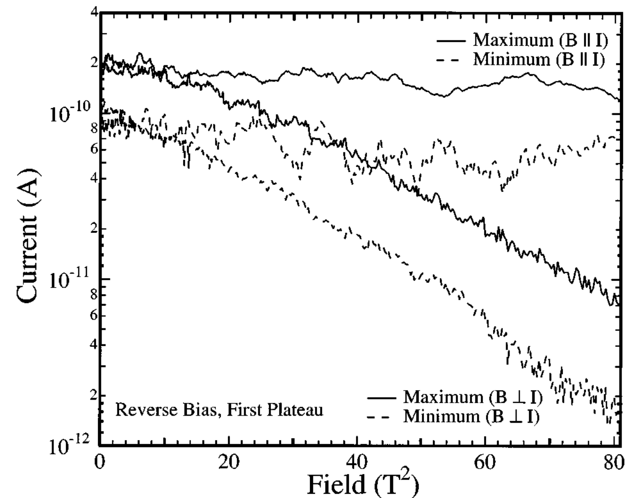


FIG. 9. Maximum (solid) and minimum (dashed) current values for the first current plateau in reverse bias as a function of perpendicular and parallel magnetic field.

Zeeman term (the term linear in $B$) in Eq. (1). Figure 7 shows a numerical calculation of the energy eigenstate dependence upon parallel magnetic field. The solid lines show the $\ell=0$ states, which exhibit only diamagnetic shifts, the dotted lines show the $\ell>0$ states.

The absence of Zeeman effects in the experimental data (i.e., peaks splitting, and shifting in energy with a linear term) implies that either we cannot probe $\ell>0$ states, possibly due to orthogonality between the emitter wave functions and $\ell>0$ dot levels, or this simply tells us that $\ell$ is not a good quantum number for this system. This implies that the assumed cylindrical symmetry has been distorted significantly. It should be noted that other groups[1,2,28] investigating similar systems also observe a diamagnetic dependence only.

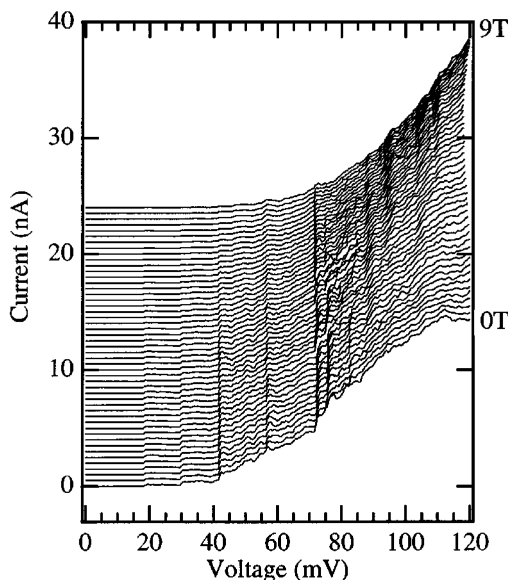


FIG. 8. Current-voltage characteristics in magnetic field perpendicular (0–9 T in 0.1825-T steps) to the current for the reverse bias direction.

As discussed earlier, for magnetic field directions perpendicular to the current, the quantum dot states should not be greatly perturbed in energy by the magnetic field ($<0.5$ meV at 10 T) due to the strong $z$ confinement. Figure 8 shows the reverse current-voltage characteristics in perpendicular magnetic field, for the same temperature and bias conditions as in Fig. 5. As expected, all of the current steps attributed to 0D dot states are not greatly affected by the perpendicular field, in contrast to the diamagnetic movement observed in the parallel field. This is confirmation that the current steps are the result of tunneling through the laterally localized dot states that reside in the strong confinement of the quantum well.

### E. Current suppression in perpendicular magnetic field

In addition to the difference in the response of the dot energy levels (i.e., the current plateau edges) to parallel and perpendicular magnetic field, suppression of the plateau current is observed for both bias directions in magnetic field oriented perpendicular to the current. Especially noteworthy are the lower plateaus in Fig. 8, which appear to vanish due to the current scale. Figure 9 shows how dramatic these effects are. Current versus magnetic field squared is shown for the maximum and minimum current observed on the first plateau in the reverse bias direction, in both parallel and perpendicular field orientations. In parallel field, the difference between the current minimum and maximum remains constant on a logarithmic scale over the field range in both bias directions, and only slight suppression is observed at 9 T. The current suppression for perpendicular field at 9 T is very large for the reverse bias (a factor of 100 for the plateau current minimum and 25 for the current maximum). In forward bias, a factor of approximately 10 is observed for both the current plateau minimum and maximum.

This current suppression has been observed previously in a coupled-dot system,[21] and was attributed to a decreasing 0D-0D transition probability between the coupled dots. In our case, since there is one quantum well, the perpendicular

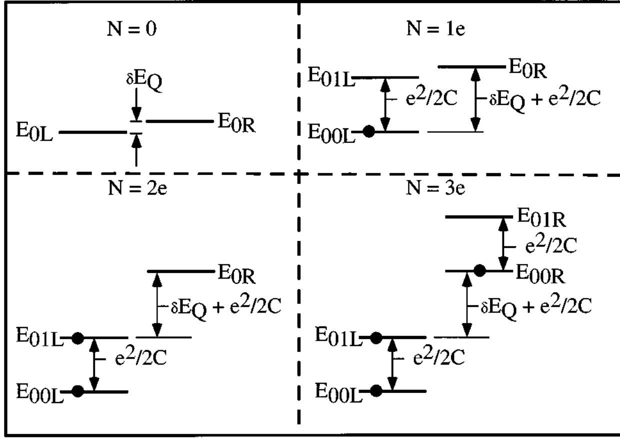


FIG. 10. Energy ladder diagram for the two dot model. For no electrons in the dot ($N$=0), there is a ground-state spin degenerate level for the left and right dot ($E_{0L}$ and $E_{0R}$), separated by a small offset, $\delta E_Q$. When the dot is occupied by one electron ($N=1e$), it will occupy the lowest state available, $E_{0L}$, and the spin degeneracy of that state will be split by the Coulomb energy, $e^2/2c$, into $E_{00L}$ and $E_{01L}$. The right state is also assumed to be lifted by the charging energy. The second electron ($N=2$) will enter the next lowest-energy state ($E_{01L}$). The third electron ($N=3$) will then enter the ground state of the right dot.

field can *only* be decreasing the 1D emitter to 0D dot transition probability. If the emitter and dot lateral wave functions are modeled as Gaussian functions, the observed linear log ($I$) versus $B^2$ trend can be accounted for. The current is proportional to the overlap between the emitter and dot wave functions,

$$I \propto \int \psi_{\text{emitter}} \psi_{\text{dot}} \, dy = \lambda \sqrt{\frac{\pi}{2}}, \tag{7}$$

where both the emitter and dot wave function are assumed to have a Gaussian wave function, $\psi \propto \exp(-y^2/\lambda^2)$. Under the application of a perpendicular magnetic field that shifts the emitter wave functions with respect to the dot wave function by a displacement $y_0$,

$$\psi_{\text{emitter}} \propto \exp[-(y-y_0)^2/\lambda^2]. \tag{8}$$

In this case,

$$\int \psi_{\text{emitter}} \psi_{\text{dot}} \, dy = \left( \lambda \sqrt{\frac{\pi}{2}} \right) \exp\left( \frac{-y_0^2}{2\lambda^2} \right). \tag{9}$$

As current is proportional to this overlap, $\log(I) \propto y_0^2$. If $y_0 \propto B$, we have the $\log(I) \propto B^2$ behavior observed experimentally.

To consider whether this trend is reasonable, note that coupling to the strong epitaxial dot potential in the $z$ direction prevents a substantial shift of the dot wave-function center.[29] The shift of the emitter wave function, $y_0$, may be estimated using the parabolic lateral potential approximation in magnetic field and assuming that in magnetic field this potential is offset by $y_0$, i.e.,

$$V = \frac{1}{2} \omega_c (y^2 - y_0^2). \tag{10}$$

TABLE II. Experimentally observed current step values in zero field and also for $B=9$ T ($B \perp I$). Suppression values are the ratio of $\Delta I_n(B=0)/\Delta I_n(B=9\ \text{T})$.

| Plateau index ($N$) | $\Delta I_n$ (pA) 0 T (−,+ bias) | $\Delta I_n$ (pA) $B=9$ T (−,+ bias) | Current suppression (−,+ bias) |
|---|---|---|---|
| 1 | 200,600 | 8,70 | 25,8.6 |
| 2 | 200,500 | 11,60 | 18,8.3 |
| 3 | 800,1100 | 80,240 | 10,4.6 |
| 4 | 2300,1600 | 500,570 | 4.6,2.8 |
| 5 | 2500,2500 | 1400,580 | 1.8,4.3 |

As a result of introducing the potential into the Hamiltonian and applying Schrödinger's equation in Cartesian coordinates, the displacement $y_0$ is given by

$$y_0 = \frac{p_z \omega_c}{m^*(\omega_c^2 + \omega_0^2)}. \tag{11}$$

For $\omega_0 > \omega_c$, this term varies as $B$, as required.

### F. Spectroscopy interpretation: The $N$-dot model

The wide bias magnetotransport studies point out some clear inconsistencies with the expected quantum dot system. The magnitude of the diamagnetic shift implies a dot wavefunction spatial extent of approximately 200 Å in diameter. For this dimension, a charging energy of 5 meV is expected,[30] and a quantization energy, $E_Q$, of 35–45 meV between the ground state and first excited state is expected (the lower limit is the parabolic result, the upper limit is the hardwall result). While the charging seems reasonable to account for the observed plateau edge to plateau edge separations (see Table I), the quantization energy is *far* too large to account for the spacing from the second to the third plateau. As the ground state is only doubly degenerate due to spin, we expect to observe only two plateaus, separated by 5 meV/$\alpha$. Subsequent plateaus in the $I(V)$ should then not be observed until at least 70 mV higher in bias. Clearly a model beyond simple charging and quantization is required to explain the experimental data.

To explain similar diamagnetic shifts in previous work, a model of conducting filaments through the dot has been proposed by Tewordt *et al.*[1] The filaments are assumed to be caused by the potential created by dopant atoms near or in the dot, which enhances the lateral quantization already present in the dot. Since on average all filament states are laterally localized by about the same amount, all of the peaks should exhibit similar diamagnetic shifts, which is observed. This also yields a more complicated density of states for the dot. However, transport through the system is still proceeding via tunneling through highly localized dot states. Note that this model also provides for the distortion of the cylindrical symmetry that is needed to prevent observation of $\ell > 0$ levels. Therefore, this model is consistent with our experimental data.

Applying this to our case, we expect to have a series of Coulomb-split plateau pairs with similar current step heights ($\Delta I_n$), current suppression (for $B \perp I$), and diamagnetic

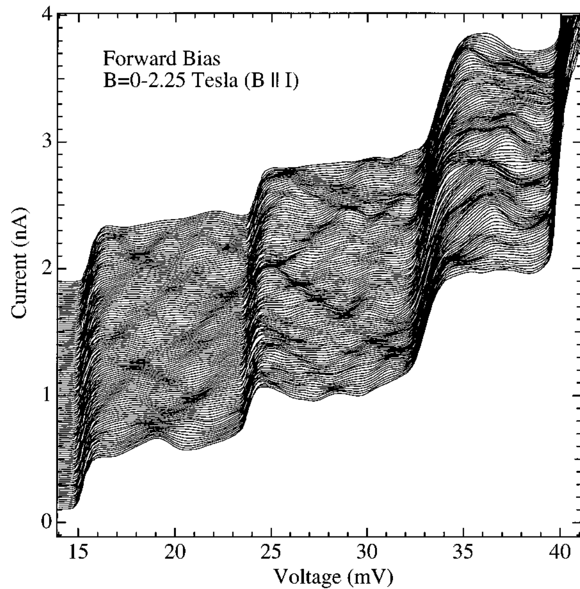


FIG. 11. $I(V)$ data in parallel field, ranging from 0 T (bottom) to 2.25 T (top). Curves are vertically offset by a constant current value for clarity.

shifts. Restated, the transport model is that conduction is proceeding through $N$ dots in parallel with the emitter. For this specific sample, $N \approx 2-3$. In examining Table I, note that for reverse bias the diamagnetic shift is the same for $N=(1,2)$ and for $N=(3,4)$, and that the energy spacing between all of these is close to what is expected for the charging energy. In the forward bias, a similar trend is observed for the $N=(1,2)$ and $N=(4,5)$ pairs. Figure 10 shows the conceptual energy ladder diagram for this transport process.

The current suppression and current step height ($\Delta I_n$) for these pairs should also track together. Table II lists the approximate $\Delta I_n$ at 0 and 9 T ($B \perp I$) and suppression values for reverse and forward bias for the first five plateaus. There is some degree of uncertainty in estimating $\Delta I_n$, as the assumption is that each current plateau is independent of the others, and that the background line shape (caused by the preceding plateaus) is flat. This approximation begins to break down around the fourth plateau in both bias directions. For the $N=(1,2)$ pairs in both bias directions, there is good agreement between both the $\Delta I_n$ values and the suppression. For the $N=(3,4)$ pair in reverse bias and the $N=(4,5)$ pair in forward bias, the agreement is not as good, although as previously mentioned there is great uncertainty in $\Delta I_n$ in this regime. However, it is interesting to note that for the $N=3$ plateau in forward bias (which exhibits a large diamagnetic shift compared to the other steps) exhibits a suppression value different from the other pairs. This could indicate that it is the result of a third dot; however, its absence in reverse bias cannot be explained. While the $N$-dot model cannot be proven conclusively with this data, it is consistent with many of the features observed (i.e., state separation, magnetic field dependence, current suppression, and the lack of Zeeman shifts).

### G. Magnetoconductance of the fine structure

While the magnetotunneling data presented in Sec. IV D allows for tracking the motion of the plateau edges in field, the magnetic field steps are too large to observe the magnetic field dependence of the fine structure occurring on the current plateaus. In order to better characterize this fine structure, data were acquired in the low bias regime (approximately ± 45 mV), every 187.5 G from 0 to 9 T. Data were acquired in both bias directions and in both parallel and perpendicular magnetic field. Figure 11 shows a portion of this survey in the forward bias direction. The magnetic field is parallel to the current and ranges from 0 (bottom) to 2.25 T (top). The $I(V)$ traces have been vertically offset by a constant current value, so the movement of the fine structure in magnetic field is apparent. Similar fine structure behavior is observed at higher magnetic fields (up to 9 T) and in magnetic field perpendicular to the current. The fine structure characteristics are reproducible, even after thermally cycling the sample to 300 K. Note that unlike the case of plateau edges resulting from localized dot states, the fine structure exhibits motion in *both* parallel and perpendicular magnetic field orientations. Note that the field steps are an order of

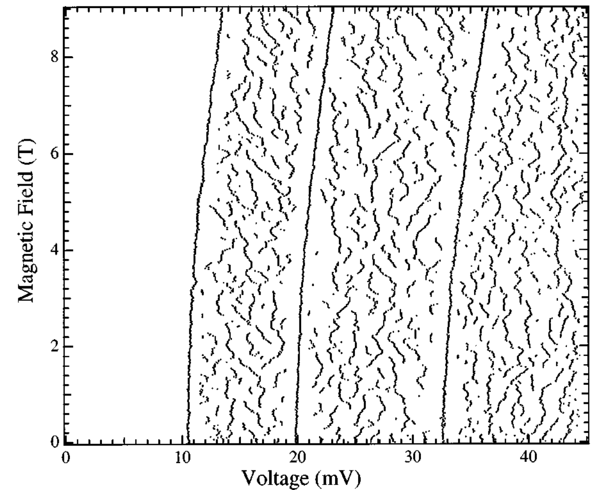


FIG. 12. Fan diagram showing peak voltage location vs magnetic field parallel to the current for the reverse bias direction.

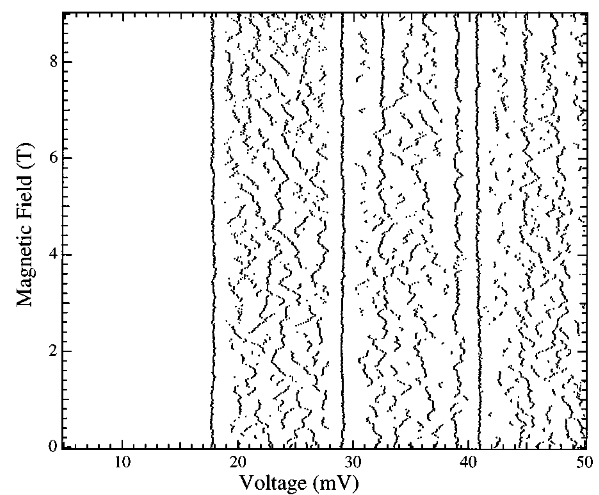


FIG. 13. Fan diagram showing peak voltage location vs magnetic field perpendicular to the current for the reverse bias direction.

TABLE III. Average fine structure peak to peak separation and standard deviation in meV.

| Plateau (bias, field) | Fine structure separation $\bar{x} \pm \sigma$ (meV) |
|---|---|
| Reverse, $B \perp I$ | $0.91 \pm 0.4$ |
| Reverse, $B \| I$ | $0.83 \pm 0.3$ |
| Forward, $B \perp I$ | $0.58 \pm 0.2$ |
| Forward, $B \| I$ | $0.81 \pm 0.3$ |

magnitude smaller than those shown in Figs. 5 and 6. It is apparent that this field dependence is different from that of the dot states. Other groups[1,2,31,32] have seen similar fine structure, however, their field steps were on the order of Tesla, rather than 100 G, so the dependence of this fine structure upon field appeared random.

To better view the data, fan diagrams were generated that plot the plateau edge and fine structure peak voltage positions versus magnetic field. Figures 12 and 13 show fan diagrams for the reverse bias in parallel field ($B \| I$) and perpendicular field ($B \perp I$), respectively. In parallel field, three lines due to the current plateau edges at 10, 20, and 32 mV ($B = 0$ T) are clearly visible. Between plateau edges, the fine structure peaks form a complex lattice of crossing lines.

For the magnetic field perpendicular to current (Fig. 13), as expected there is little motion of the stronger lines (18, 29, and 41 mV) associated with quantum dot states. While the fine structure, the number of plateaus observed, and the plateau widths are consistent through device thermal cycling, the spectra are sometimes offset in voltage. We believe this is due to the charging configuration that is in place in the emitter and collector upon cooldown, which may change from run to run.

Note how the fine structure motion in Figs. 12 and 13 clearly correlates with varying magnetic field. From measuring the slope of these lines, we find that the fine structure typically moves at a rate of 2.5 mV/T (1.25 meV/T) in reverse bias and 5.0 mV/T (1.85 meV/T) in the forward bias direction. Both of these values are on order of the value for $eB/m^*$ (1.8 meV/T in $In_{0.1}Ga_{0.9}As$ and 1.7 meV/T in GaAs). Similar field dependence of the fine structure is seen in the perpendicular orientation, in contrast to the motion of the dot state current plateau edges, which only are shifted in magnetic field parallel to current. This confirms that the source of the fine structure does not reside in the dot and strongly implies the presence of emitter states.

The average energy separation between the fine structure peaks on the first plateau in both bias and field directions has been calculated by performing a numerical Fourier transform upon the fan diagrams. Table III shows the values for the mean fine structure separation, $\bar{x}$, and the standard deviation, $\sigma$. As expected, no dramatic change in the peak separation is observed when the field orientation is changed.

In previous work by Su and Goldman,[2,31] the fine structure was observed to quench in magnetic field. This was viewed as evidence against the fine structure being attributed to a discrete density of states in the emitter. This is not the case observed for the samples studied in our work. Even at fields of up to 11 T the fine structure is still strong and clearly present. In strong perpendicular field, the fine structure is observed to quench at the *same* rate as the current steps. Both are suppressed due to a decrease in the emitter-dot transition probability in perpendicular field, and this is the expected result if the fine structure is due to the density of states in the emitter.

### H. Origin of the fine structure

Several factors indicate that the fine structure results from the emitter contact. The weak temperature dependence shows that the fine structure is not due to states in the dot and is due to tunneling processes from states below the Fermi level in the emitter. The observation of thermally activated preresonant fine structure peaks is consistent with this model. Also, recent results have shown that the fine structure is due to emitter states by studying transport in asymmetric quantum dots.[28] In these experiments, transport employing a thin emitter and a thick collector shows no fine structure, as the smaller collector transmission coefficient controls the tunneling current. In the reverse bias direction, when injecting from the collector, the fine structure is observed. This clearly indicates that the fine structure is dependent upon the injection contact and is only observable when injection contact controls the tunneling current. In our symmetric structure, we observe the fine structure in *both* bias directions, as expected. The observation that the fine structure is generally more pronounced in the reverse bias is also expected. The voltage to energy conversion factor, $\alpha$, for the reverse bias is slightly larger than $\alpha$ for forward bias. This implies that the emitter is *thicker* for the reverse bias and *thinner* for the forward bias, which is consistent with the extreme case presented in Ref. 28. The motion of the fine structure in magnetic field, which is on the order of $\hbar \omega_c$, is consistent with what one expects for states in GaAs when the confinement energy is weak. The lack of dependence upon magnetic field orientation excludes states localized in the dot, as states in the dot exhibit very different response in parallel ($B \| I$) versus perpendicular ($B \perp I$) magnetic field orientations due to the strong quantum-well confinement.

The observed fine structure peak energy separations of 0.6–0.9 meV are too small to arise from 1D subbands in the leads. For a 1400-Å-wide lead, the 1D subbands are calculated to be separated by 15 meV near the Fermi level. Even if the lead diameter is increased to 3400 Å (much larger than the possible fabrication upper limit of approximately 1500 Å) the calculated energy spacings are still 5 meV.

Other possible models to account for this close energy separation, including interference effects,[33] universal conductance fluctuations (UCF),[34] or effects due to chaotic transport[35] can be individually excluded. Interference effects require sharp corners in the lateral potential, which we do not expect, and predict much larger values for the energy separation of the fine structure than is observed (on order 50 meV). UCF effects are expected to show a random motion in magnetic field, not the monotonic dependence upon field that is exhibited by the fine structure. Additionally, the observation of a thermally activated peak, the lack of a strong temperature dependence of the fine structure, and the observation of the fine structure at temperatures greater than 10 K also make UCF effects unlikely as an explanation for the fine structure. The localization extent of the dot states makes any chaotic trajectories inside the dot unlikely as well.

The small energy separation between the fine structure peaks in conductance indicates that they may be due to the effect that individual donors have upon the 1D density of states in the emitter. For the dopant levels used in this structure, there are approximately two impurities in a 100-Å cube in the emitter (the value of 100 Å is used as it is the mean free path in the doped lead at low temperature). This places about 100 dopant atoms with electrons contributing to the degenerate doping of the conduction band in this volume. For a calculated Fermi level of 80 meV, this results in level spacings that are approximately 0.8 meV in energy (2.2 mV in forward bias, 1.6 mV in reverse bias). This in good agreement with the observed 0.6–0.9-meV spacing. Another possibility is to assume that fluctuations in the 1D emitter lead cause localization in the $z$ direction (current direction). While this could be occurring, it is still difficult to obtain energy spacings of 0.6–0.9 meV from this effect without increasing the localization length to very large values (i.e., $>3400$ Å). To investigate the responsible process further, samples with different dopant levels and spacer layer thicknesses could be fabricated to conclusively determine if the fine structure energy spacing is related to the discrete dopants.

## V. CONCLUSIONS

The electron spectroscopy of a quasi-0D vertical $In_{1-x}Ga_xAs$ quantum dot resonant tunneling structure is investigated as a function of magnetic field and temperature. Steps in current due to the discrete nature of the dot density of states are observed. In magnetic field parallel to the current, the step edges exhibit a diamagnetic shift as expected. The magnitude of this diamagnetic shift is used as a direct measure of the radial extent of the wave function in the dot. In the magnetic field perpendicular to current, no shift is observed, which conclusively shows that the current steps are due to states localized in the epitaxial quantum well. Suppression of the current plateaus is observed only for magnetic fields perpendicular to the current, and is found to be consistent with a decreasing overlap between emitter and dot wave functions. The inconsistencies in the step spacings, the diamagnetic shifts, and lack of Zeeman splittings indicate that transport is proceeding through more than one channel in parallel (i.e., two dots, or more). A model incorporating this type of transport is proposed and found to be consistent with the first few plateaus.

Using the highly localized dot states as spectroscopic probes, the electronic structure of the emitter electrode is measured through the oscillatory fine structure observed on top of the normal current plateaus. The fine structure modulates with a period of 0.6–0.9 meV and is observed to be reproducible, both upon repeated traces and upon thermal cycling. Variable temperature results indicate that this fine structure originates from below the Fermi level in the emitter. With increasing temperature, states *above* the Fermi level are populated. The observation of preresonant thermally activated peaks as temperature increases is in excellent agreement with the emitter discrete state model. In both parallel and perpendicular magnetic field orientations, the fine structure peaks shift at approximately $\hbar\omega_c = 1.7$ meV/T, which is again consistent with emitter states. The most likely physical origin for the observed fine structure is the random dopant distribution in the emitter contact.

## ACKNOWLEDGMENT

The authors would like to acknowledge the support of the Office of Naval Research for this work.

[*]Present address: Digital Semiconductor, 77 Reed Road, M/S HLO 2-3/J9, Hudson, MA, 01752.

[†]Present address: Department of Materials Science and Engineering, University of Wisconsin at Madison, Madison, WI, 53706.

[1] M. Tewordt *et al.*, Phys. Rev. B **46**, 3948 (1992).

[2] B. Su, V. Goldman, and J. Cunningham, Phys. Rev. B **46**, 7644 (1992).

[3] M. Reed *et al.*, Phys. Rev. Lett. **60**, 535 (1988); M. Reed *et al.*, Festköperprobleme **29**, 267 (1989).

[4] M. Dellow *et al.*, Electron. Lett. **27**, 134 (1991).

[5] S. Tarucha, Y. Hirayama, T. Saku, and T. Kimura, Phys. Rev. B **41**, 5459 (1990); S. Tarucha and Y. Hirayama, *ibid.* **43**, 9373 (1991).

[6] U. Meirav, M. Kastner, and S. Wind, Phys. Rev. Lett. **65**, 771 (1990).

[7] P. McEuen *et al.*, Phys. Rev. Lett. **66**, 1926 (1991).

[8] L. Kouenhoven *et al.*, Z. Phys. B **85**, 367 (1991); **85**, 381 (1991).

[9] A. Ramdane, G. Faini, and H. Launois, Z. Phys. B **85**, 389 (1991).

[10] J. H. Luscombe, Nanotechnology **4**, 1 (1993).

[11] H. Liu and G. Ayers, J. Appl. Phys. **65**, 4908 (1989).

[12] G. Bryant, Phys. Rev. B **39**, 3145 (1989).

[13] H. van Houten and C. Beenakker, Phys. Rev. B **63**, 1893 (1989).

[14] D. Averin, A. Korotkov, and K. Likharev, Phys. Rev. B. **44**, 6199 (1991).

[15] Y. Meir, N. Wingreen, and P. Lee, Phys. Rev. Lett. **66**, 3048 (1991).

[16] A. Groshev, T. Ivanov, and V. Valtchinov, Phys. Rev. Lett. **66**, 1082 (1991).

[17] L. Chen and C. Ting, Phys. Rev. B **44**, 5916 (1991).

[18] N. Johnson and M. Payne, Phys. Rev. Lett. **67**, 9 (1991).

[19] P. Mooney, Festköperprobleme **29**, 215 (1989).

[20] The conduction band profiles in Figs. 1(a) and 1(b) are numerically calculated using the method outlined in W. R. Frensley, Superlattices Microstruct. **11**, 347 (1992).

[21] M. Tewordt *et al.*, Phys. Rev. B **49**, 8071 (1994).

[22] G. Oliviera *et al.*, Phys. Rev. B **35**, 2896 (1987).

[23] In Ref. 1, the expression for capacitance incorrectly includes a factor of $4\pi$ in the denominator. $E_C$ is given as $e^2/C$, whereas it should be $e^2/2C$.

[24] V. Goldman, D. Tsui, and J. Cunningham, Phys. Rev. B **35**, 9387 (1987).

[25] T. Ericsson and A. Ruhe, Math. Comput. **35** (12), 1251 (1980).

[26] M. Tewordt *et al.*, in *Proceedings of the 20th International Conference on the Physics of Semiconductors*, edited by J. Joannopoulos (World Scientific, Singapore, 1991), p. 2455.

[27] V. Fock, Z. Phys. **47**, 446 (1928); C. Silorski and U. Merkt, Phys. Rev. Lett. **62**, 2164 (1989); W. Hansen *et al.*, *ibid.* **62**, 2168 (1989).

[28] T. Schmidt *et al.*, Phys. Rev. B **51**, 5570 (1995).

[29] If the wave function in the dot shifted significantly, the confinement energy would also change, which is not seen experimentally (i.e., no plateau shift for magnetic field perpendicular to current).

[30] In estimating the charging energy, $E_C$, the crucial parameter is the junction area. The geometrical capacitance argument assumes a metallic density of states, which is a questionable assumption in the emitter and collector electrodes, and certainly suspect in the dot. To provide a better estimate, a charging radius $R_C$ is assumed. $R_C$ is estimated from the wave-function extent determined from the diamagnetic shift (100 Å), which results in $E_C \approx 5.0$ meV.

[31] V. Goldman, B. Su, and J. Cunningham, in *Nanostructures and Mesoscopic Systems* (Academic, San Diego, 1992), pp. 173–182.

[32] M. Tewordt *et al.*, Solid-State Electron. **37**, 793 (1994).

[33] G. Bryant, Phys. Rev. B **44**, 12 837 (1991); A. Szafer and A. D. Stone, Phys. Rev. Lett. **62**, 300 (1989).

[34] A. D. Stone, in *Physics and Technology of Submicron Structures* (Springer, Berlin, 1988), p. 108.

[35] R. A. Jalabert, H. Baranger, and A. D. Stone, Phys. Rev. Lett. **65**, 2442 (1990); T. Fromhold *et al.*, Surf. Sci. **305**, 511 (1994); Phys. Rev. Lett. **72**, 2608 (1994).